Solid State Communications 250 (2017) 92–98

Contents lists available at ScienceDirect

Solid State Communications

journal homepage: www.elsevier.com/locate/ssc

Communication

Effect of crystal morphology on magnetic structure of nano-magnetites

Y.H. Chen*, J.F. Zhang

Department of Earth Sciences, National Cheng Kung University, 1, University Rd., East Dist., Tainan City 701, Taiwan, ROC

ARTICLE INFO

Keywords:
A. Nano-magnetite
C. Morphology
D. Magnetic property
E. Magnetic force microscopy

ABSTRACT

The nano-magnetites with particle, rod, tube, and ring crystal morphologies were synthesized and the differences between macroscopic and microscopic magnetic properties were studied. The macroscopic magnetic properties of nano-magnetites obtained via a superconducting quantum interference device (SQUID) showed that both coercive magnetic field and saturation magnetization per unit volume followed the orders of ring > particle > tube > rod, respectively. This indicated that the crystal morphology affected macroscopic magnetic properties. The particle nano-magnetite contained a single domain while the others contained multiple domains measured by a magnetic force microscope (MFM). However, the domain structure of nano-magnetites calculated from SQUID data showed that all were pseudo-single domains. This suggested that the MFM may be a precise tool to determine magnetic structures. Moreover, the crystal morphology of nano-magnetites affected magnetic properties owing to different magnetic-domain structures.

1. Introduction

The variation of geomagnetism on geological timescales relies on the recovery of paleomagnetic signals of magnetic minerals from rocks and sediments. Therefore, it is imperative to reveal the formation and recording mechanisms, as well as fidelity, of the magnetic minerals [1]. Viscous magnetization is a general time-dependent component of natural remanent magnetization (NRM), and is known to importantly affect the reliability of paleomagnetic results. Understanding viscous magnetization processes and the controlling mechanisms is very useful to paleomagnetism [2]. Iron oxides (magnetite, maghemite, titanomagnetite) and iron sulfides (greigite, pyrrhotite) are common magnetic minerals, and are important carriers of magnetic remanence of the rocks.

To realize the contribution of these magnetic minerals to geomagnetics, several studies have focused on synthetic magnetic nano-minerals and investigated their magnetic properties. For example, Williams et al. [3] used a three-dimensional finite element/boundary integral micromagnetic model to discuss the crystal morphology effect on the magnetic structure and magnetic stability of nanomagnetites. Their results imply that morphological complexities endow magnetite nanoparticles with an enhanced coercivity. Chen et al. [4] have studied the magnetic properties of cubic and octahedral nanomagnetites and the materials exhibit ferromagnetic behavior; however, the cubic Fe_3O_4 particle shows a smaller coercive magnetic field (H_c) because of its higher symmetry and smaller shape anisotropy compared to the octahedral Fe_3O_4 particle. Morphological control of metal oxide nanocrystals is a fascinating subject because magnetic properties of these materials are largely dependent on their crystal shape [5–8]. The crystal morphology of magnetic minerals could affect their magnetic properties and magnetic structure and further influence their magnetic ability or thermomagnetic measurements. Therefore, the magnetic domain structure of magnetic minerals offers clues

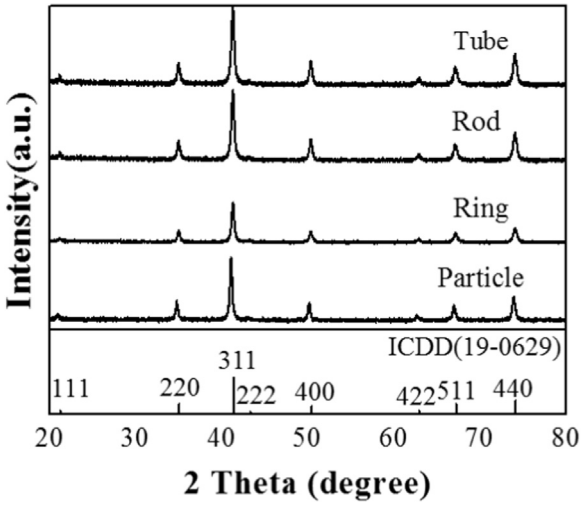

Fig. 1. The XRD pattern of nano-magnetites with different crystal morphologies.

* Corresponding author.
E-mail address: yhc513@mail.ncku.edu.tw (Y.H. Chen).

http://dx.doi.org/10.1016/j.ssc.2016.11.021
Received 10 August 2016; Received in revised form 23 September 2016; Accepted 25 November 2016
Available online 25 November 2016
0038-1098/

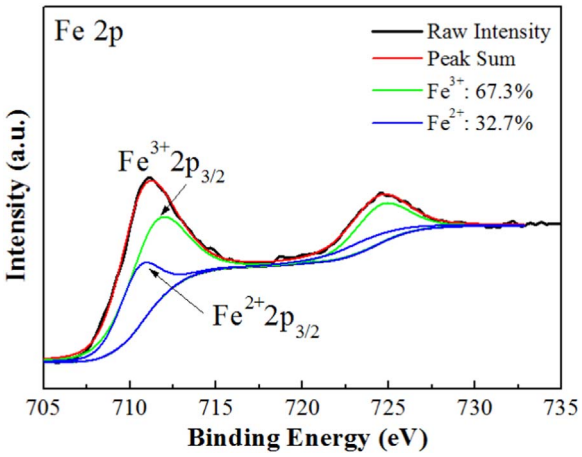

Fig. 2. The Fe $2p_{3/2}$ peaks in XPS spectra for the nano-magnetite.

for analyzing geomagnetics.

The magnetic force microscopy (MFM) is a powerful tool for investigating the magnetic structure with excellent lateral and vertical resolutions of approximately 25 nm and 1 nm, respectively [9,10]. The MFM can effectively detect and localize the magnetic fields arising from magnetic domains of magnetic nano-minerals. MFM images are formed by scanning the attractive and repulsive magneto-static fields with interactions between the magnetic tip in the vertical direction and the surface of a sample in the horizontal direction. If the magnetization of a sample is oriented along the vertical direction (z-axis) and the tip can be represented as a magnetic dipole with magnetization along the z-axis, the shifts are shown on the MFM images by dark and bright areas where the field is formed. Thus, positive shifts (repulsion) are bright, while negative shifts (attraction) are dark [10–12]. Frandsen et al. [10] used MFM to investigate the spatial distribution of magnetic domains in micro-magnetites for fully understanding the magnetic properties of rocks at microscopic and macroscopic scales. Shaar

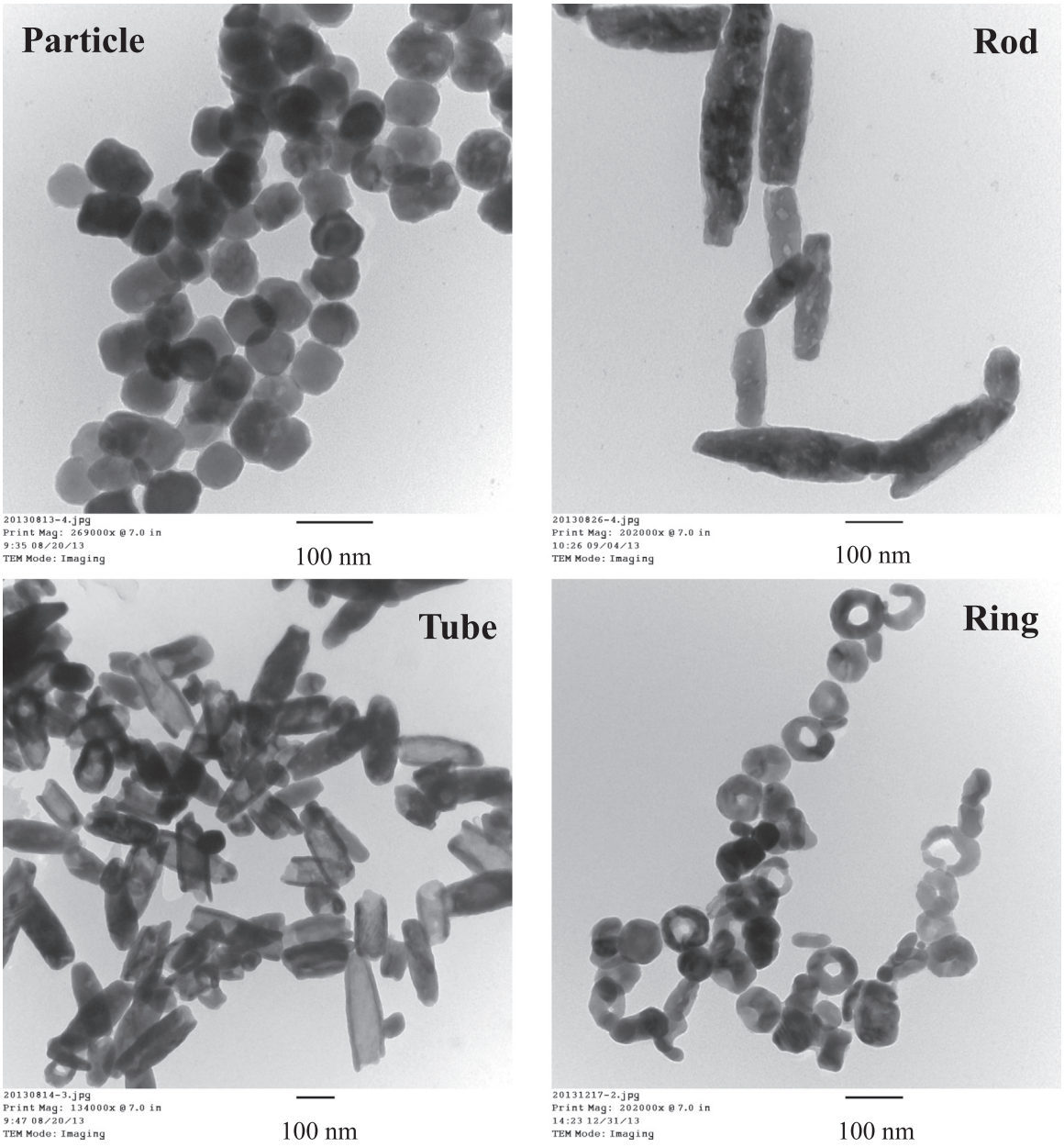

Fig. 3. TEM images of magnetites with (a) nanoparticle-, (b) nanorod-, (c) nanotube-, and (d) nanoring-like morphologies.

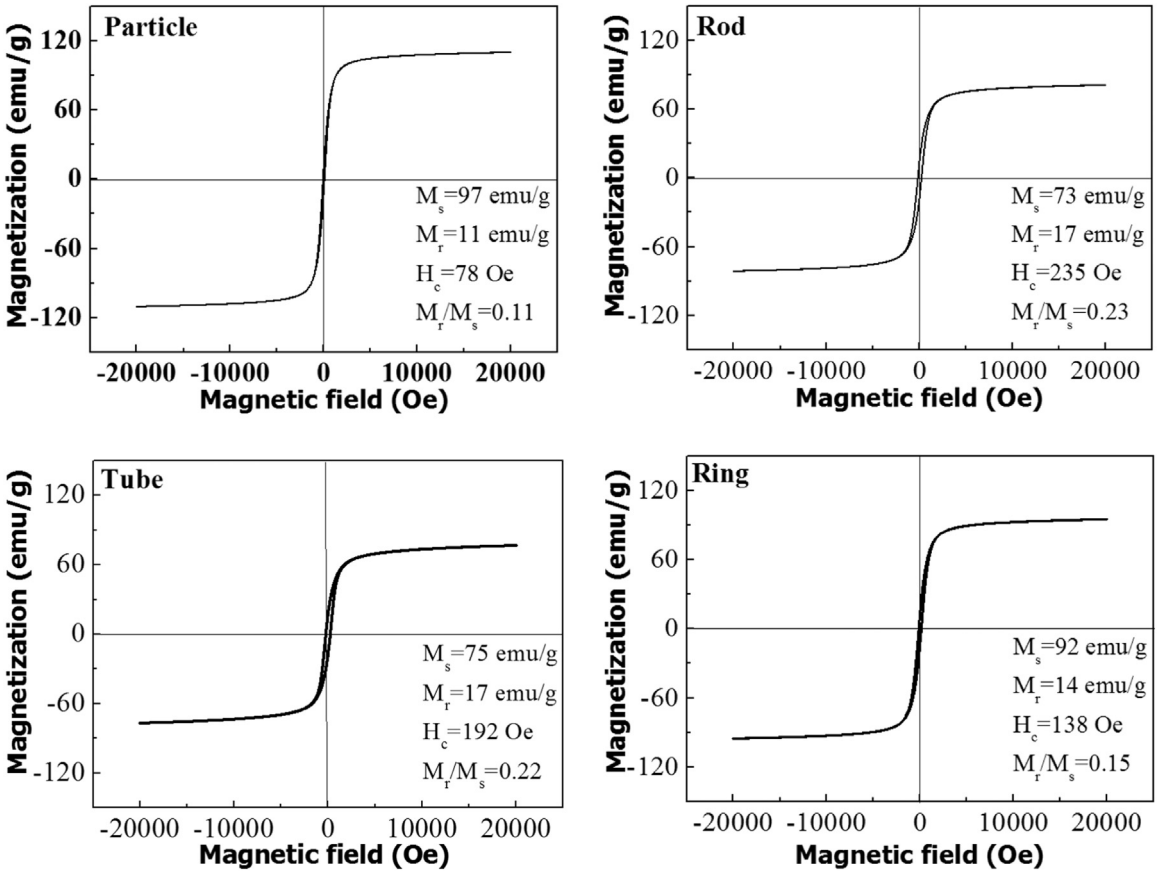

Fig. 4. Magnetization plots as a function of magnetic field of nano-magnetites with various crystal morphologies.

and Feinberg [13] used MFM to study the magnetic properties of dendritic rocks with basaltic glass composition to gain insights from MFM images for paleomagnetic studies. Furthermore, submicroscopic magnetite particles from highly shocked granite-gneisses close to the core of the Vredefort impact structure have been investigated using MFM (Cloete et al. [14]). Therefore, MFM images are helpful in identifying simple magnetic-domain configurations.

Nano-magnetites in mid-ocean ridge basalts (MORB) and submicron-scale greigite (pyrrhotite) in sedimentary rocks play important roles in geomagnetics [15–18]. Because nano-magnetites and nano-greigite usually contain single or pseudo-single magnetic domains, they are magnetic carriers and may be contributors to the natural remanent magnetization abnormality. In this paper, nano-magnetites with particle, rod, tube, and ring crystal morphologies are synthesized. This study aims to demonstrate the application of MFM to investigate magnetic characteristics of domain structures in individual grains. We show how this technique can help determine the internal domain configuration of the nano-magnetites with different crystal morphologies and map their possible magnetic stray fields. Finally, the mechanism of magnetism in nano-magnetites with different crystal shapes are discussed, and macroscopic and microscopic magnetism are compared.

2. Material and methods

Nano-magnetites with particle, rod, tube, and ring morphologies were synthesized using a hydrothermal method to initially fabricate nano-hematites [19–22] and then the nano-hematites subsequently extracted via a carbon reduction method [23,24] to obtain our nano-magnetite samples. The morphology and grain size of the nano-magnetites were observed using transmission electron microscopy (TEM, H-7500, Netherlands). The crystal structures of nano-magnetite powders were characterized through X-ray powder diffraction analyses ($Cu_{k\alpha}$, Bruker, D8 Advance, Germany). X-ray photoelectron spectroscopy (XPS, PHI 5000 Versa Probe) was employed to confirm the oxidation state of iron ions in the nano-magnetites.

The macroscopic magnetism was measured using a superconducting quantum interference device (SQUID, Quantum Design, USA) magnetometer at room temperature with a magnetic field of up to 1 T. The microscopic analysis of the magnetic structures was performed through magnetic force microscope (MFM, Innova AFM, Bruker, USA), in which the radius of curvature of the magnetic tips was approximately 20 nm. The instrument was operated in the combination of tapping and lift modes. The resonance frequency of the cantilevers was ~75 kHz, and the height of the tip above the sample was set to ~50 nm.

3. Results

Fig. 1 shows the X-ray diffraction patterns of the magnetite crystals with the nanoparticle-, nanorod-, nanotube-, and nonoring-like morphologies. All crystal types showed a cubic structure and this result was in agreement with the standard data given in the International Centre for Diffraction Data (ICDD) card for magne-

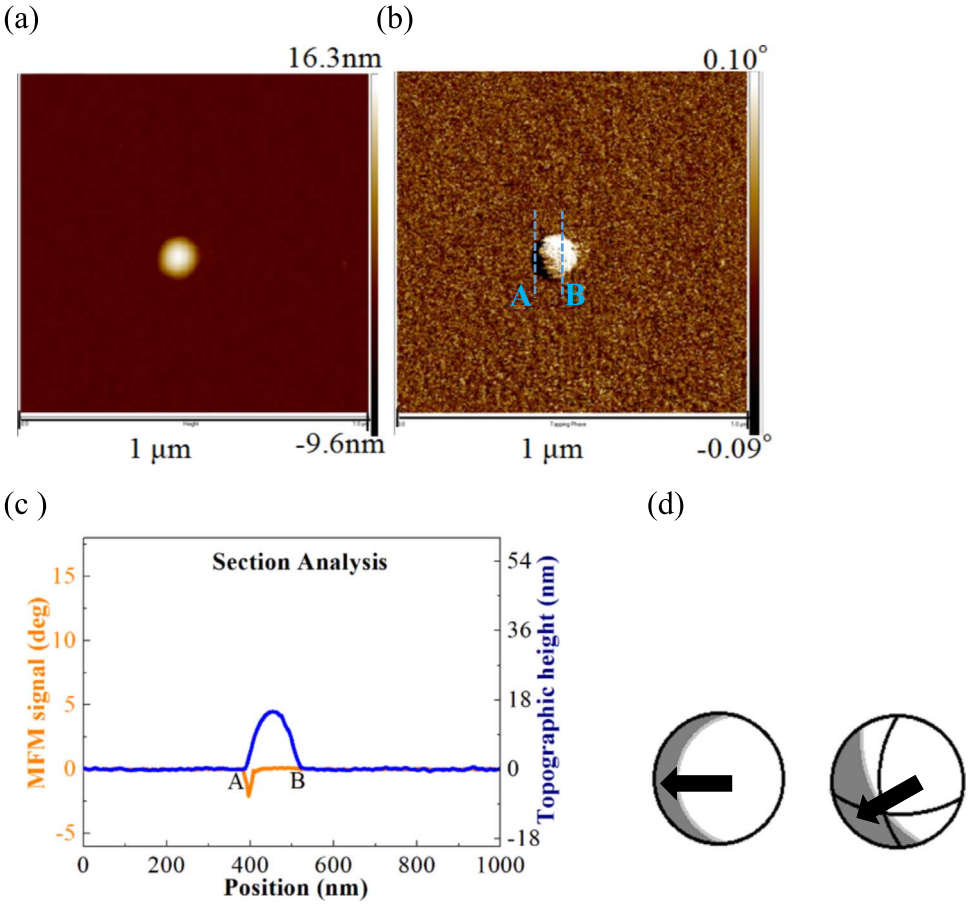

Fig. 5. The MFM images of (a) topography, (b) amplitude, (c) magnetic-signal, and (d) the magnetic structure of magnetite nanoparticles.

tites (19–0629). Moreover, the diffraction peaks of all the samples were strong and sharp, indicating that well-crystallized nano-magnetites of various morphologies could be obtained using the simple synthesis processes.

The oxidation states of iron ions in the nano-magnetite (here shows particle-like nano-magnetite) were determined using X-ray photoelectron spectroscopy as Fe(II) and Fe(III) with a resolution of approximately 0.2 eV in the measured binding energy. The Fe $2p_{3/2}$ spectra for nano-magnetite were fitted using the method reported by Grosvenor et al. [25]. As shown in Fig. 2, both the Fe(II) and Fe(III) species were clearly observed in the nano-magnetite samples.

The morphologies and particle sizes of the nano-magnetites were investigated using TEM (Fig. 3). The crystals of the nanoparticles were granular, and the particle sizes were in the range of 45–85 nm. The nanorods were acicular; the widths and lengths of their crystals were in the ranges of 50–100 nm and 250–350 nm, respectively. The nanotubes were tube shaped; their crystals had inner and outer diameters in the ranges of 40–85 nm and 80–110 nm, respectively, and lengths in the range of 150–300 nm. The nanorings consisted of crystals with an inner diameter of 20–45 nm, an external diameter of 70–100 nm, and the height around 25 nm.

The SQUID measurement revealed that all the nano-magnetite crystals exhibited ferrimagnetic behavior (Fig. 4); the coercive magnetic fields of the nanoparticles, nanorods, nanotubes, and nanorings were 78, 245, 192, and 138 Oe, respectively, and the saturation magnetizations (M_s) of the nanoparticles, nanorods, nanotubes, and nanorings were 97, 73, 75, and 92 emu/g, respectively. The microscopic magnetic structure could be estimated using the ratio of remanent magnetization (M_r) to M_s, as proposed by Dunlop [26]. The values of M_r/M_s of nanoparticles, nanorods, nanotubes, and nanorings were 0.11, 0.23, 0.22, and 0.15, respectively. These values could be classified into the pseudo single-domain type.

Figs. 5(a)–(c) showed the MFM topography and amplitude images, and magnetic-signal of magnetite nanoparticles, respectively. In the amplitude image, the entire nanoparticle presented a small black-area (A) and a large bright-area (B). In the magnetic-signal (Fig. 5(c)), the nanoparticle exhibited a negative MFM signal, which is characteristic of a single domain. Fig. 5(d) presented the possible magnetic structure, which indicates that the magnetite nanoparticle is a magnetic carrier with a single domain and the arrow means the magnetic direction of N pole.

Figs. 6(a)–(d) exhibited the MFM topography, amplitude, and magnetic signal images in addition to the magnetic structure of the magnetite nanorods. In the amplitude image, a bright area appeared in the middle zone, however, a black area occurred in the lateral zone. This phenomenon was also observed in the magnetic-signal image, in which the bright area had a stronger magnetization than the black area did. The magnetic-signal image indicated characteristics of multiple domains. The possible magnetic structure (Fig. 6(d)) was that the spin direction is perpendicular to the axial orientation of the nanorod, which has multiple magnetic domains.

In the case of the nanotube (Figs. 7(a)–(d)), the bright area (A and D) appeared in the lateral zones; however, black (B) and weakly black (C) areas occurred in the middle zones (Fig. 7(b)). This phenomenon agreed with the magnetic-signal image, in which the

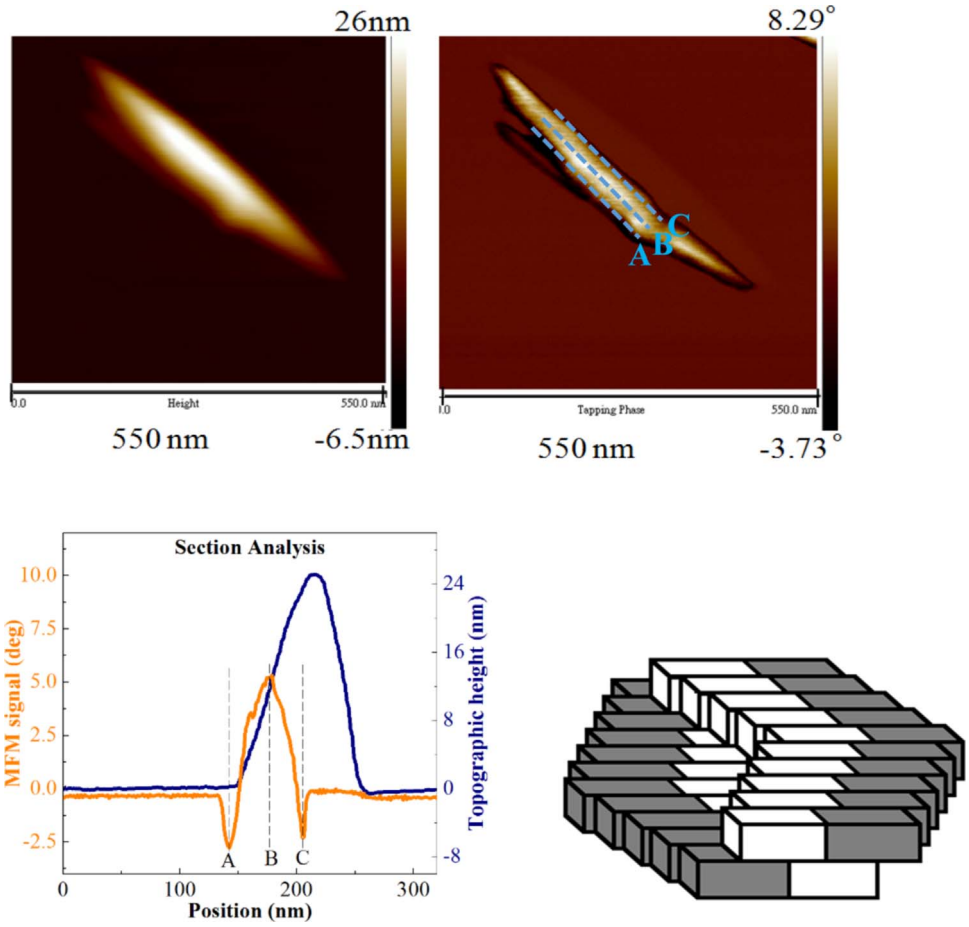

Fig. 6. The MFM images of (a) topography, (b) amplitude, (c) magnetic-signal, and (d) the spin distributions of magnetite nanorods.

bright area A had stronger magnetization than the other areas did. The possible magnetic structure of magnetite nanotube was shown in Fig. 7(d). The magnetic structure was similar to that reported by Kazakova et al. [27]; the spin direction was along the axial orientation of the nanotube and exhibited a closed-loop magnetic structure, which is characteristic of multiple magnetic domains.

In the MFM images of the magnetite nanorings (Figs. 8(a)–(d)), the topographic height of B be a little lower due to that it is in the center of the ring and the bright areas appeared along with the dark areas. This agreed with the magnetic signal image in which the distribution of the bright areas of A, B, and C were oriented along the orbital direction. The possible magnetic structure of the magnetite nanoring was shown in Fig. 8(d). The structure was characteristic of a multi-domain and the spin direction was along the orbital orientation of the nanoring. The presence of multiple domains in minerals is related to the saturation magnetization. The net magnetic energy increases with increasing saturation magnetization; thus, the magnetic domain walls occurred to decrease the magnetic energy [28].

4. Discussion

From the SQUID results, the coercive magnetic field and saturation magnetization followed the orders of nanoparticle < nanoring < nanotube < nanorod and nanoparticle > nanoring > nanotube > nanorod, respectively, which implies that the crystal morphology can affect the macroscopic magnetic property. The magnetic properties are related to factors such as the size, morphology, structure, and so on. Our nano-magnetite samples have the same crystal structure; therefore, the effect of crystal structure on the magnetic properties is negligible. In order to eliminate the “size effect”, the coercive magnetic field (saturation magnetization) per unit volume of the nanoparticles, nanorods, nanotubes, and nanorings were 5.4×10^{-4} (6.7×10^{-4}), 1.8×10^{-4} (5.5×10^{-5}), 2.1×10^{-4} (8.3×10^{-5}), and 1.1×10^{-3} (7.6×10^{-4}) Oe·nm^{-3} (emu·g^{-1}·nm^{-3}), respectively. The estimated volume of the nanoparticle, nanorod, nanotube, and nanoring is $4/3\times\pi\times r^3$, $\pi\times r^2\times L$, $\pi\times(r_1^2-r_2^2)\times L$, and $\pi\times(r_1^2-r_2^2)\times h$, respectively. The r means the radius of nanoparticles (32.5 nm) and nanorods (37.5 nm); L is the length of nanorods (300 nm) and nanotubes (225 nm); $r_1$and $r_2$are the outer and inner radii of nanotubes (47.5/31.25 nm) and nanorings (42.5/16.25 nm); h means the height of nanorings (25 nm); the abovementioned parameters are obtained from TEM results (Fig. 3). This indicated that the nanorings exhibited the highest coercive magnetic field. Thus, the magnetic properties are related to the effect of shape anisotropy. Magnetic domains and domain walls are two important related concepts to the magnetization process of ferromagnetic materials. The changes in domain wall motion and domain rotation processes are the principal reasons for the alteration in the magnetic polarization. The important factor of realizing magnetically soft materials is the convenience of domain wall movement. As a result, a small coercivity is the consequences of the small potential energy barriers to domain wall motion [29]. This phenomenon is due to the

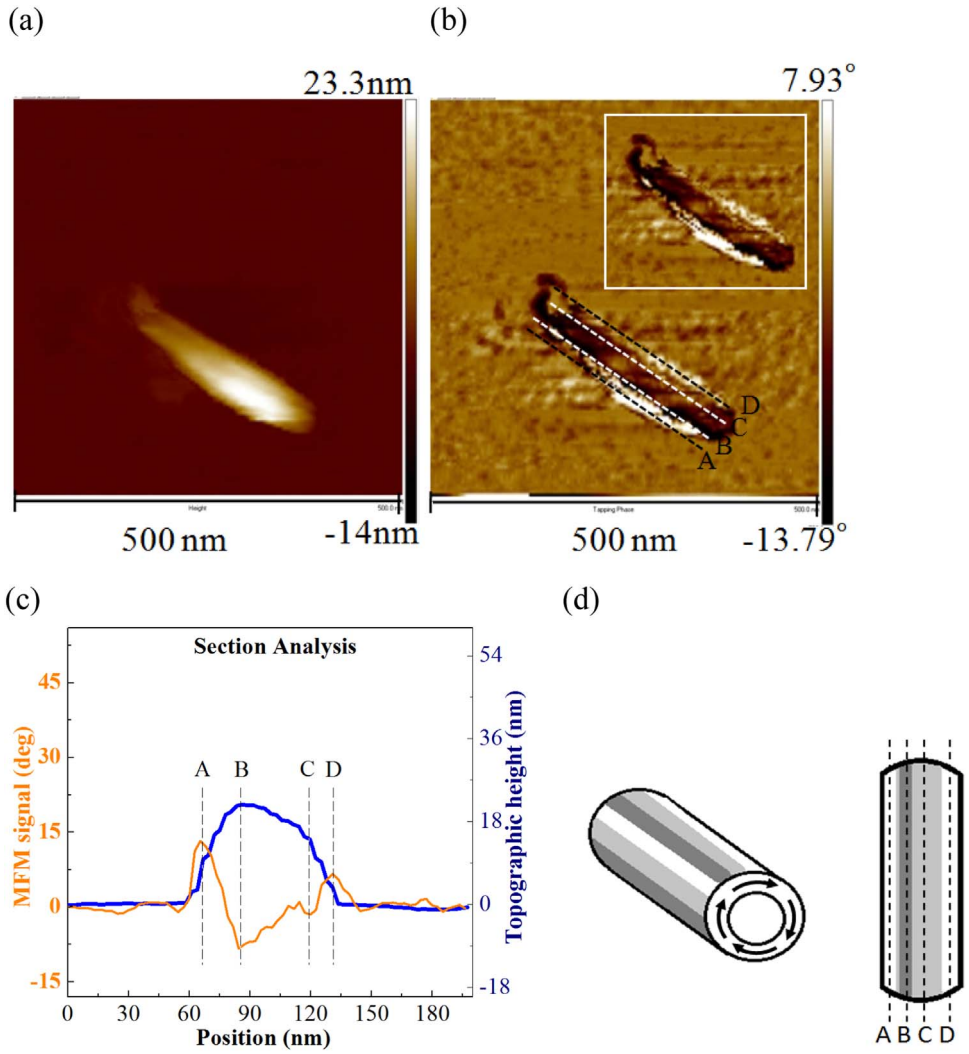

Fig. 7. The MFM images of (a) topography, (b) amplitude, (c) magnetic-signal, and (d) the magnetic structure of magnetite nanotubes.

magnetic-domain structure. To change the magnetization of a multiple-domain sample, its domain wall must be translated, which is an energetically simple process; however, to change the magnetization of a single-domain specimen, it needs to rotate the entire magnetization, which is an energetically consuming process [30]. As for the magnetite nanoparticle, it has a single magnetic domain; thus it is more difficult to rotate the entire magnetization. Consequently, it has a larger coercive magnetic field. The magnetite nanoring has the highest coercive magnetic field, which may be owing to a more complicated magnetic domain structure (spin distribution) among all the samples. Therefore, the morphology of nano-magnetites affects their magnetic properties (magnetic domain type and spin canting), which is in keeping with those reported previously [31–35].

The domain structure estimated from SQUID data indicated that all nano-magnetite morphologies had pseudo-single domains. However, the MFM images indicated that the nano-particle had a single domain, while the others had multiple domains, which suggests that MFM may be a more powerful and precise tool to determine the magnetic structure at the microscopic scale (It is real showing the magnetic distribution of the magnetic sample). The crystal morphology of the nano-magnetites affects their magnetic properties, both at the macroscopic and microscopic levels, which indicates that the natural remanent magnetism abnormality of MORB may be considered an effect of the morphology of magnetic minerals. Moreover, the MFM may be useful to reveal the correlation between the microscopic and macroscopic magnetic properties of magnetic minerals.

5. Conclusions

We synthesized nano-magnetites with particle, rod, tube, and ring crystal morphologies and studied their macroscopic and microscopic magnetic properties using SQUID and MFM, respectively. The results indicate that the crystal morphology of nano-magnetites can influence their magnetic properties both at the macroscopic and microscopic levels. The magnetic-domain structures determined using SQUID were different from those determined using MFM images, which suggests that the MFM investigation may be more precise than the SQUID measurements for a microscopic magnetic propertires. The magnetic recording fidelity for geomagnetics should be considered as the microscopic magnetic characteristics of magnetic minerals, and the MFM technique can be used as a powerful tool for determining the magnetic structure. This study provides an example of the possible applications of MFM and its potential to contribute to the correlation between microscopic scale features and the macroscopic magnetic proper-

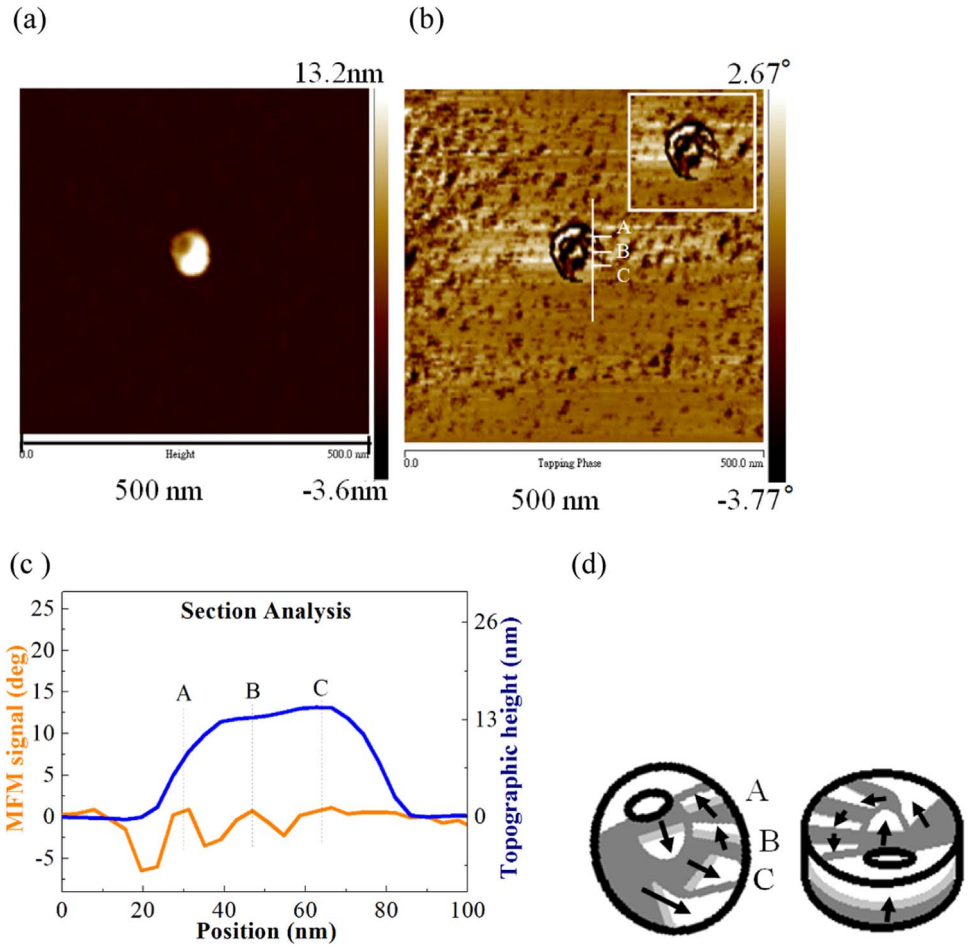

Fig. 8. The MFM (a) topography, (b) amplitude, (c) magnetic-signal, and (d) the magnetic stray fields of magnetite nanorings.

ties of magnetic minerals.

Acknowledgments

The authors would like to thank the Instrument Center of National Cheng Kung University for the SQUID measurement. We also thank to students and research assistant in Science and Technology Lab of Department of Earth Sciences for information collection. We sincerely thank to the Ministry of Science and Technology for the financial support.

References

[1] T.P. Almeida, A.R. Muxworthy, W. Williams, T. Kasama, R. Dunin-Borkowski, Geochem. Geophys. Geosyst. 15 (2014) 161–175.
[2] A.R. Muxworthy, W. Williams, J. Geophys. Res. 11 (111) (2006) B01103–B01115.
[3] W. Williams, M.E. Evans, D. Krása, Geochem. Geophys. Geosyst. 11 (2) (2010). http://dx.doi.org/10.1029/2009GC002828.
[4] R.F. Chen, J.H. Cheng, Y. Wei, J. Alloy. Compd. 520 (2012) 266–271.
[5] Y.H. Tong, Y.C. Liu, C.L. Shao, J. Phys. Chem. B 110 (2006) 14714–14718.
[6] X.H. Hu, J.C. Yu, J.M. Gong, Adv. Mater. 19 (2007) 2324–2329.
[7] Z.Y. Huo, C.K. Tsung, W.Y. Huang, Nano Lett. 9 (2009) 1260–1264.
[8] H.J. Song, N. Li, S.L. Yu, Micro Nano Lett. 5 (4) (2010) 200–202.
[9] C. Frandsen, S.L.S. Stipp, S.A. McEnroe, M.B. Madsen, J.M. Knudsen, Phys. Earth Planet Inter. 141 (2004) 121–129.
[10] Bruker, The Operation Manual, 2011.
[11] H. Takahoshi, H. Saito, S. Ishio, J. Magn. Magn. Mater. 272–76 (2004) e1313–e1315.
[12] J. Santoyo-Salazar, M.A. Castellanos-Roman, L. Beatriz-Gómez, Mater. Sci. Eng. C. 27 (2007) 1317–1320.
[13] R. Shaar, J.M. Feinberg, Geochem. Geophys. Geosyst. 14 (2013) 407–421.
[14] M. Cloete, R.J. Hart, H.K. Schmid, M. Drury, C.M. Demanet, K.V. Sankar, Contrib. Miner. Petrol. 137 (1999) 232–245.
[15] C.S. Horng, C. Lai, T.Q. Lee, J.C. Chen, Terr. Atmos. Ocean. Sci. 3 (1992) 519–532.
[16] C.S. Horng, M. Torii, K.S. Shea, S.J. Kao, Earth Planet Sci. Lett. 164 (1998) 467–481.
[17] W.T. Jiang, C.S. Horng, A.P. Roberts, D.R. Peacor, Earth Planet Sci. Lett. 193 (2001) 1–12.
[18] C.S. Horng, A.P. Roberts, Earth Planet Sci. Lett. 241 (2006) 750–762.
[19] H.M. Fan, G.J. You, Y. Li, Z. Zheng, H.R. Tan, Z.X. Shen, S.H. Tang, Y.P. Feng, J. Phys. Chem. C 113 (2009) 9928–9935.
[20] B. Lv, Y. Xu, Q. Gao, D. Wu, Y. Sun, J. Nanosci. Nanotechnol. 10 (2010) 2348–2359.
[21] L. Song, S. Zhang, B. Chen, J. Ge, X. Jia, Colloids Surf. A 360 (2010) 1–5.
[22] Y. Xu, S. Yang, G. Zhang, Y. Sun, D. Gao, Y. Sun, Mater. Lett. 65 (2011) 1911–1914.
[23] H. Wang, P. Hu, D. Pan, J. Tian, S. Zhang, A.A. Volinsky, J. Alloy. Compd. 502 (2010) 338–340.
[24] P. Hu, S. Zhang, H. Wang, D. Pan, J. Tian, Z. Tang, A.A. Volinsky, J. Alloy. Compd. 509 (2011) 2316–2319.
[25] A.P. Grosvenor, B.A. Kobe, M.C. Biesinger, N.S. Mclntyre, Surf. Interface Anal. 36 (2004) 1564–1574.
[26] D.J. Dunlop, J. Geophys. Res. 107 (2002) B3. http://dx.doi.org/10.1029/2001IJB000486.
[27] O. Kazakova, M. Hanson, A.M. Blixt, B. Hjorvarsson, J. Magn. Magn. Mater. 258–259 (2003) 348–351.
[28] E.E. Carpenter, J. Magn. Magn. Mater. 225 (2001) 17–20.
[29] D. Sellmyer, R. Skomski, Advanced Magnetic Nanostructures, Springer, New York, 2006, pp. 491–496.
[30] L.Y. Zhang, Y.F. Zhang, J. Magn. Magn. Mater. 321 (2009) L15–L20.
[31] C.W. Han, S.H. Lim SH, J. Phys. D 42 (2009) (045006–1~045006–5).
[32] J.Y. Zhong, C.B. Cao, Sens. Actuators B 145 (2010) 651–656.
[33] J.M. Gu, S.H. Li, M.L. Ju, J. Cryst. Growth 320 (2011) 46–51.
[34] W.C. Zhu, X.L. Cui, L. Wang, T. Liu, Q. Zhang, Mater. Lett. 65 (2011) 1003–1006.
[35] A. Bouremana, A. Guittoum, M. Hemmous, D. Martínez-Blanco, J.A.B. Pedro Gorria, N. Benrekaa, Mater. Chem. Phys. 160 (2015) 435–439.